Surface Engineering

ISSN: 0267-0844 (Print) 1743-2944 (Online) Journal homepage: https://www.tandfonline.com/loi/ysue20

Effects of heat treatment on HVOF-sprayed Fe-based amorphous coatings

Chunyan Li, Haibo Wang, Juanqiang Ding, Shunping Wang, Jinling Li & Shengzhong Kou

To cite this article: Chunyan Li, Haibo Wang, Juanqiang Ding, Shunping Wang, Jinling Li & Shengzhong Kou (2020): Effects of heat treatment on HVOF-sprayed Fe-based amorphous coatings, Surface Engineering, DOI: 10.1080/02670844.2020.1759936

To link to this article: https://doi.org/10.1080/02670844.2020.1759936

Published online: 13 May 2020.

SURFACE ENGINEERING
https://doi.org/10.1080/02670844.2020.1759936

The Institute of Materials, Minerals and Mining

Taylor & Francis
Taylor & Francis Group

Effects of heat treatment on HVOF-sprayed Fe-based amorphous coatings

Chunyan Li[a,b], Haibo Wang[b], Juanqiang Ding[b], Shunping Wang[b], Jinling Li[b] and Shengzhong Kou[a,b]

[a]State Key Laboratory of Advanced Processing and Reuse of Nonferrous Metals, Lanzhou University of Technology, Lanzhou, Gansu, People's Republic of China; [b]School of Materials Science and Engineering, Lanzhou University of Technology, Lanzhou, Gansu, People's Republic of China

ABSTRACT

In this study, Fe-based amorphous coatings were fabricated on 304 stainless steel by high-velocity oxyfuel (HVOF). Moreover, the properties of Fe-based amorphous coatings heat-treated at 150°C and 250°C were investigated. The XRD analysis shows that the structure of heat-treated amorphous coatings is all amorphous, and the porosity of heat-treated amorphous coatings is lower than that of original amorphous coatings. With the heat-treated temperature increasing, the corrosion resistance of amorphous coatings is improved in artificial seawater. Compared with the original coatings, the heat-treated amorphous coatings have great creep resistance. The wear resistance of heat-treated amorphous coatings is excellent than original amorphous coatings in artificial seawater and dry friction condition. The experiment results point out that the heat-treated amorphous coatings have excellent properties, which can improve properties of Fe-based amorphous coatings.

ARTICLE HISTORY
Received 7 February 2020
Revised 28 March 2020
Accepted 19 April 2020

KEYWORDS
High-velocity oxyfuel; Fe-based amorphous coatings; heat-treated amorphous coatings; corrosion resistance; creep resistance; wear resistance

Introduction

Fe-based bulk metallic glass (BMG) exhibits excellent mechanical, physical and chemical properties, such as high strength, soft magnetic, excellent corrosion resistance, making BMG have broad application prospect [1–3]. However, most BMG cannot be used as structural material, because its plasticity at room temperature is poor and exhibiting brittle fracture. In order to handle this issue, Fe-based amorphous powder can be prepared on the surface of rollers, gears and drills, etc. to form the coatings by thermal spraying [4]. Thermal spraying technology is considered to be a major advance in metal surface protection [5,6].

Fe-based amorphous coatings can be fabricated by high-velocity oxyfuel (HVOF), and the properties have been studied. Miura et al. [7] first fabricated a variety of Fe-based amorphous coatings using flame spraying techniques, and the amorphous sheet of the $Fe_{40}Ni_{40}P_{14}B_6$ alloy with about 150 μm in thickness can be prepared. Wang et al. [8] discovered that the spray distance can greatly affect the shape and structure of the amorphous coatings, and too long or too short spray distance was not conducive to the amorphous coatings. The amorphous alloy of $Fe_{47.14}Cr_{16.36}Mo_{30.84}C_{3.76}B_{1.90}$ obtained a completely amorphous structure and the lower porosity at a spray distance of 200 mm. The corrosion resistance of Fe-based amorphous coatings prepared by Branagan et al. [9] using HVOF technology was directly proportional to the amorphous content, and the corrosion resistance was due to the improved addition of elements of Cr, Mo and W [10]. Wu et al. [11] found the relationship between spray particles and porosity and obtained the low-porosity coatings by HVOF with the spray particles of 20–30 μm. Zhang et al. [12] fabricated the Fe-based amorphous coating of $Fe_{53}Cr_{19}Zr_7Mo_2C_{18}Si_1$ by HVOF. The coating was completely amorphous and had good corrosion resistance in 3.5% NaCl solution. However, the amorphous coating was partially crystallized at 750°C during annealing, which reduces the corrosion resistance. Qin et al. [13] obtained Fe-based amorphous coating with dense structure and excellent corrosion resistance by optimizing spraying parameters. By seeking a reasonable spray distance, air flow and spray power, the coating porosity can be reduced, the amorphous content in the coating can be increased, and the corrosion resistance of the coating can be increased. Li et al. [14] used nanoindentation to study the creep behaviour of Fe-based amorphous coatings at room temperature. At different peak load and load-holding time, the creep displacement increased a little and tends to be stable, indicating that creep deformation more sensitive to the applied peak load compared withholding time.

In this paper, Fe-based amorphous coatings were fabricated by HVOF on 304 stainless steel. The heat treatment method below the glass transition temperature is used to reduce the porosity of the amorphous coatings and improve the atomic relaxation state. Moreover, the defects of the amorphous coatings prepared by

CONTACT Chunyan Li licywz@163.com State Key Laboratory of Advanced Processing and Reuse of Nonferrous Metals, Lanzhou University of Technology, Lanzhou, Gansu 730050, People's Republic of China; School of Materials Science and Engineering, Lanzhou University of Technology, Lanzhou, Gansu 730050, People's Republic of China

HVOF are reduced with the method. The corrosion resistance, creep resistance and wear resistance of the amorphous coatings are studied with the method which expands the application of Fe-based amorphous coatings in the field of industrial protection.

Experimental materials and methods

Fe-based alloy powder (25.0–27.0 wt-% Cr, 16.0–18.0 wt-% Mo, 2.0–2.5 wt-%C, 2.0–2.2 wt-% B, and the balance Fe) provided by Guangzhou Wandun Amorphous Trading Co. Ltd. was used. The 304 stainless steel with a size of 10 × 10 × 10 mm was used as the substrates. It was cleaned and sprayed with Al_2O_3 particles before spraying. The Fe-based amorphous coatings were fabricated by Meike's DJ-2700 HVOF spraying system as shown in Figure 1. The system used N_2 as powder delivery gas, and O_2 as combustion-supporting, the flow rate of O_2 was 19m^3 h^{-1}, the powder feed rate was 22 g min^{-1}, the spraying distance was 280 mm, the flow rate of kerosene was 8 L h^{-1}, and the traverse velocity of the spray gun was 800 mm s^{-1}. Fe-based amorphous coatings were prepared on 304 stainless steel with above process parameters as shown in Figure 1 (inset). The amorphous coatings were heat-treated for 30 min at 150°C and 250°C by the heat treatment furnace (KSL-1200X) and insulated the air with magnesium oxide powder.

The structures were detected by X-ray diffraction (XRD, D/max-2400, Cuk_α). The thermal behaviour was determined by differential scanning calorimeter (DSC, Netzsch STA-449C) at a heating rate of 10° C min^{-1} from 25 to 1000°C. The microstructure of the surface, the cross-section, the corrosion surface, and the wear surface of amorphous coatings were observed by scanning electron microscope (SEM, JSM-6700F), and the amorphous coatings heat treated at 250°C in dry friction condition element types and contents were detected by the Energy Dispersive Spectrdmeter (EDS, JSM-6700F). The porosity of the amorphous coatings was measured by using Image J. Electrochemical corrosion tests were performed in artificial seawater by an electrochemical workstation (CHI660E), and the dynamic polarization curves were scanned at a fixed rate of 1 mV s^{-1}. Nanoindentation experiments were carried out on the amorphous coating surface with Hysitron TI-950 nanoindentation instrument, and the peak load was 6 and 10 mN with the constant load rate of 0.8 mN s^{-1} and the loading time of 10, 20 and 30 s. The creep deformations of the TI-950 friction head were observed by an Atomic Force Microscope (AFM) to analyse the indentation morphology. The wear tests were carried out at room temperature with different environments (dry friction and artificial seawater) by a wear tester (MFT-R4000), and the commercially available GCr15 steel balls (6 mm diameter) were used as friction pairs. The slide stroke was 5 mm, the sliding frequency was 5 Hz, the friction and wear time was 30 min, and the load was 20 N. The surface morphology, wear scar roughness and wear volume of the specimen were analysed by a non-contact optical profiler (MicroXAM-800) manufactured by KLA-Tencor, USA.

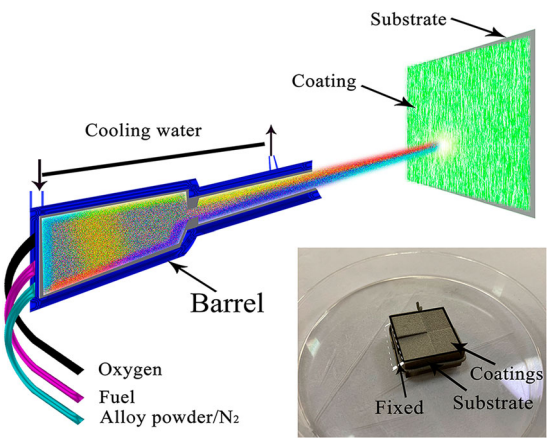

Figure 1. Schematic of high velocity oxyfuel and specimens of Fe-based amorphous coatings (inset).

Results and analysis

Structure and microstructure of the amorphous coatings

The DSC curve displays the crystallization temperature (T_x = 301.85°C) and the glass transition temperature (T_g = 251.85°C), which are the basis of selecting the heat treatment temperature in this paper, as shown in Figure 2(a). The heat treatment temperature is selected as 250°C and 150°C which are below T_g. Figure 2(a) (inset) exhibits the SEM morphology of Fe based amorphous powder. It is clearly seen that the surfaces of majority powders are spherical and smooth with diameters of 16–54 um, which are beneficial to the spraying. The cross-sectional morphology of the original amorphous coatings is shown in Figure 2(b). The original amorphous coatings with thickness around 100 um adhere well to the substrates and have a dense structure, which consists of layered regions and the typical amorphous coatings structure by the method of HVOF. Figure 2(c) shows the X-ray diffraction pattern of the powder, original amorphous coatings and the heat-treated amorphous coatings. It can be seen from the spectrum that the shapes of the four curves are no obvious crystal diffraction peak, which indicates that the powder and amorphous coatings are completely amorphous structure.

Porosity of the amorphous coatings

The cross-sectional microstructure of the original amorphous coatings and heat-treated amorphous coatings were observed by SEM, as shown in Figure 3. It is

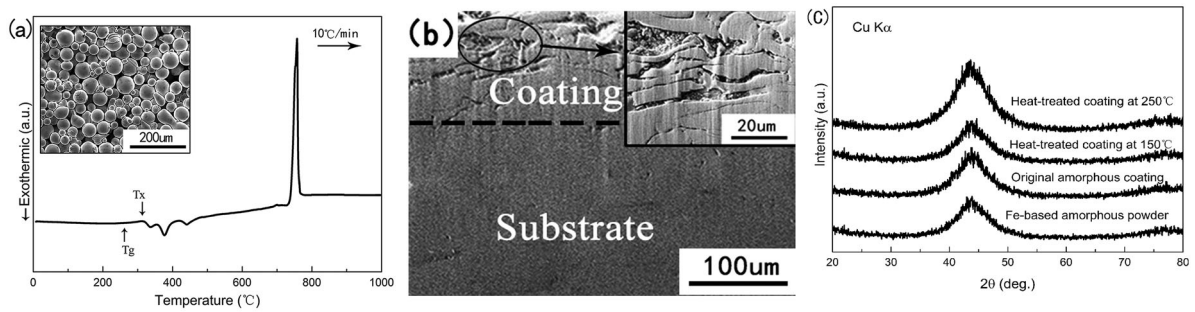

Figure 2. (a) DSC analysis of original amorphous coatings and SEM micrograph of amorphous powders (inset); (b) SEM cross-sectional micrograph of original amorphous coatings; (c) XRD pattern of powder and amorphous coatings.

found that there are some finite pores on the surface of the amorphous coating. Owing to the rapid cooling characteristics of HVOF, the semi-fused particles shrink during the spraying process, which causes some finite pores on the amorphous coatings. With the increase of the heat treatment temperature, the porosities of the amorphous coatings decrease, and the porosity is 1.7% in Figure 3(a), 0.9% in Figure 3(b) and 0.5% in Figure 3(c), respectively. The results indicate that solid atoms diffuse in a reordered arrangement and submerge some of the pores in the amorphous coatings, resulting in a drop of amorphous coating porosity, when amorphous coatings are annealed at a low temperature without crystallization [15,16].

Corrosion property of the amorphous coatings

The electrochemical test is the most common, simple and intuitive method used to study the corrosion resistance of a specimen. It measures the corrosion resistance of the material by the current and potential of the working electrode. The self-corrosion current density I_{corr} and the self-corrosion potential E_{corr} are obtained by the extrapolation of Tafe curves, and polarization resistance R_p can be calculated according to the following formula [17]:

$$R_p = \frac{\beta_\alpha \beta_c}{2.303 I_{corr}(\beta_\alpha + \beta_c)} \tag{1}$$

where β_a and β_c are the slopes of the linear polarization regions of the anode and cathode polarization, respectively. The polarization resistance R_p indicates the equivalent resistance of per unit area of the specimen during the transfer of the charge at the electrode/solution interface. The R_p is the higher, the corrosion rate is the lower [18]. The self-corrosion current density I_{corr} can be used to characterize the magnitude of the corrosion rate. According to Faraday's law, the amount of material precipitated or dissolved on the electrode is Δ m.

$$\Delta m = \frac{AIt}{nF} \tag{2}$$

where A is the atomic weight of the metal; I is the current intensity; t is the energization time; n is the valence of the metal, and F is the Faraday constant. For uniform corrosion, the entire metal surface area S can be regarded as the anode area, so the corrosion current density can be described:

$$I_{corr} = \frac{I}{S} \tag{3}$$

So, the corrosion rate can be determined:

$$V = \frac{\Delta m}{St} = \frac{A}{nF} \times I_{corr} \tag{4}$$

Therefore, the corrosion rate $V \propto I_{corr}$, and the larger the I_{corr} is, the greater corrosion rate the material is. The self-corrosion current density I_{corr} and polarization resistance R_p of the substrates and the amorphous coatings in the artificial seawater etching solution are calculated by the above formula.

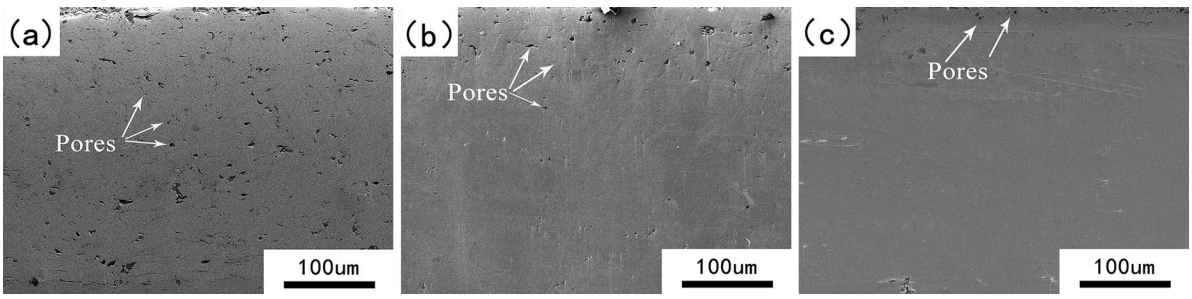

Figure 3. Cross-sectional morphology of the amorphous coatings: (a) Original amorphous coatings; heat-treated amorphous coatings at 150°C (b) and 250°C (c).

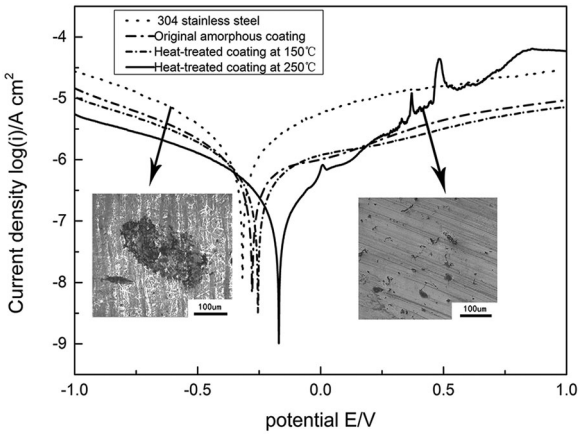

Figure 4. Potentiodynamic polarization curves in artificial seawater of substrates, original amorphous coatings and amorphous coatings heat-treated at 150°C and 250°C.

Figure 4 shows the polarization curves of substrates, original amorphous coatings and heat-treated amorphous coatings in artificial seawater. As heat treatment temperatures increase, the corrosion current densities decrease, which indicates that corrosion resistance becomes better. The corrosion area is small and a few corrosion pits appear for the heat-treated coatings at 250°C. However, many corrosion areas are generated for 304 stainless steel substrates, and SEM images are inserted in Figure 4. The corrosion potentials are $E_{corr250°C} > E_{corr150°C} > E_{corr\ original\ coatings} > E_{corr\ substrates}$, corrosion current densities are $I_{corr250°C} < I_{corr150°C} < I_{corr\ original\ coatings} < I_{corr\ substrates}$ and polarization resistances are $R_{p250°C} > R_{p150°C} > R_{p\ original\ coatings} > R_{p\ substrates}$, as shown in Table 1. It can be concluded that the amorphous coatings have better corrosion resistance than the substrates, and the amorphous coatings heat treated at 250°C has great corrosion resistance.

The amorphous coatings contain some elements which have strong passivation ability, such as Cr [19]. These elements can form a dense, stable and complete passive film on the surface of the amorphous coatings, such as Cr_2O_3, which is firmly bonded to the amorphous coatings as a protective barrier of the substrates. Owing to the characteristics of HVOF, pores are produced in the amorphous coatings, and the porosity has a great influence on the corrosion resistance of Fe-based amorphous coatings. The surface free energy at the pore position is relatively larger than other areas, and most of the various interface phenomena are caused by the existence and change of the interface free energy. Moreover, the stability of the passivation film on the surface is affected, and the tendency of the passivation film on the surface of the coatings to crack is also greatly increased [20]. As the heat treatment temperatures increase, the porosities of the amorphous coatings decrease, and the stability of the passivation film increases, so the corrosion resistance of the amorphous coatings improves.

Table 1. Parameters from potentiodynamic polarization curves of amorphous coatings.

Specimen	E_{corr}/V	I_{corr}/($A{\cdot}cm^{-2}$)	R_p/($\Omega{\cdot}cm^{-2}$)
Substrates	−0.313	16.029E-7	13,624.585
Original amorphous coatings	−0.262	12.339E-7	559,006.341
Heat-treated amorphous coatings at 150°C	−0.276	10.368E-7	252,340.943
Heat-treated amorphous coatings at 250°C	−0.213	37.777E-8	337,289.849

Nanoindentation analysis of the amorphous coatings

C. Y. Li et al. [14] analysed the creep behaviour of the original amorphous coatings at different load-bearing times with peak loads of 6 and 10 mN. The loading rate was 0.8 mN s^{-1} and the load-holding time was 10, 20 and 30 s. It can be known that under the peak load of 6 and 10 mN, the creep displacement will increase rapidly during the initial creep stage with the increase of the load-holding time, and the increase will decrease when the load-bearing time reaches 20 s. Finally, it was gradually approaching stable.

Figure 5 exhibits creep displacement curves at different holding times of heat-treated amorphous coatings at 150°C and 250°C under 6 and 10 mN loading conditions, respectively. The heat-treated amorphous coatings have a lesser increase in creep displacement than the original amorphous coatings, and are less sensitive to the holding time than the original amorphous coatings, indicating the heat-treated amorphous coatings have better creep resistance. This phenomenon can be attributed to the structural relaxation of the amorphous coatings during heat treatment, which can eliminate defects (initial free volume) in the amorphous coatings [15]. More atoms will participate in the deformation process under the indentation, and the heat-treated amorphous coatings have a greater creep resistance during the holding stage.

Figure 6 illustrates the observation of pile-ups of the amorphous coatings heat-treated at 150°C (a) and 250°C (b) caused by shear band expansion with atomic force microscopy (AFM) at peak load of 10 mN with holding time of 30 s. It can be concluded that indentation creep may lead to the formation and expansion of multiple shear regions around the material, which may lead to the material softening [21].

Friction and wear properties of the amorphous coatings

SEM analysis of wear morphology

Figure 7(a–c) show the wear morphology of 304 stainless steel and the original amorphous coatings with the wear time of 30 min and the load of 20 N in artificial seawater and the wear morphology of

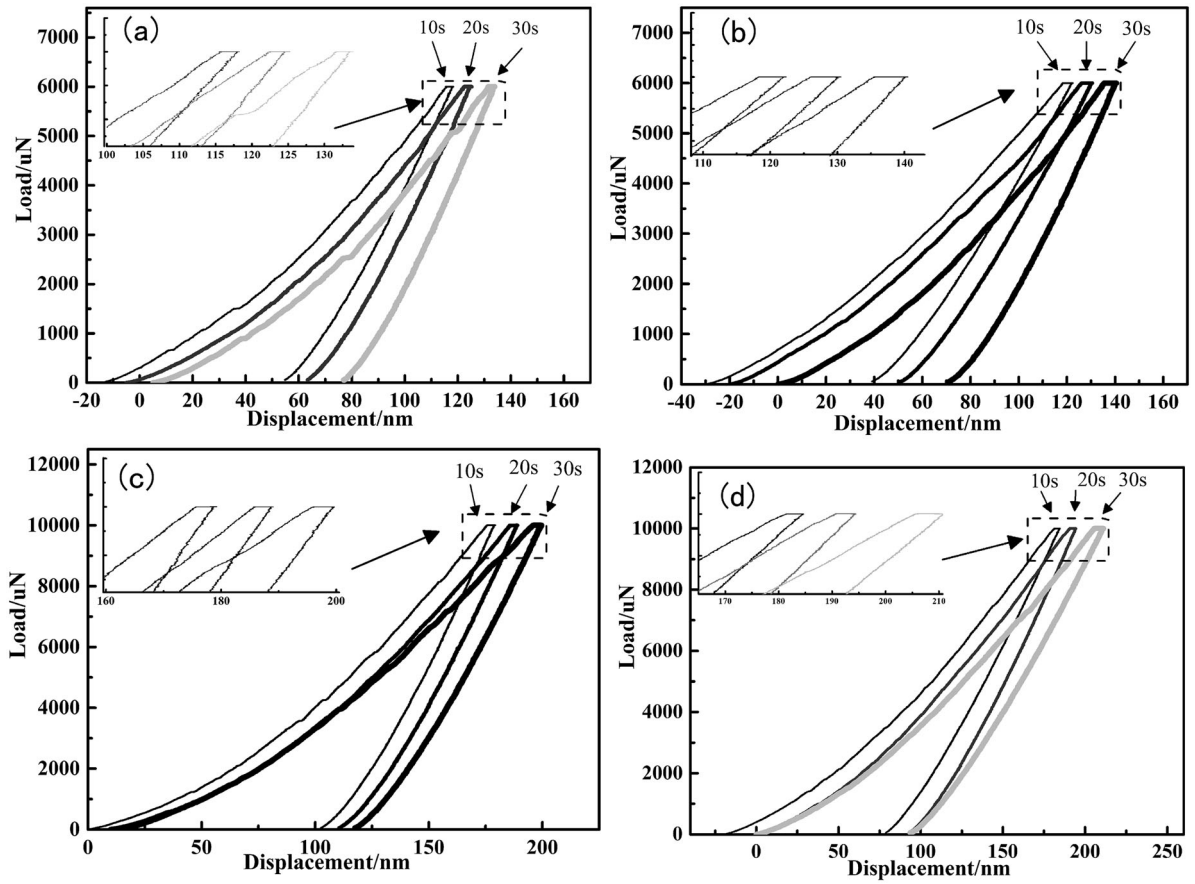

Figure 5. Load-creep displacement curves at different holding times of amorphous coatings: heat treated at 150°C (a) and 250°C (b) under 10 mN loading condition; heat treated at 150°C (c) and 250°C (d) under 6 mN loading condition.

the original coatings with the wear time of 30 min and load of 20 N in dry friction condition. After the surface of 304 stainless steel is worn, there are more irregular abrasive particles, and there is a tendency of delamination. It shows that the micro-cutting effect of the abrasive particles, the main wear mechanism is abrasive wear [22]. Compared with the wear trajectory of 304 stainless steels, there are few spalling and abrasive particles, and the partial oxidation appears on the surface of original amorphous coatings. The main wear mechanism of original amorphous coatings is abrasive wear and oxidative wear, but the oxidative wear of original amorphous coatings is more severe under dry friction conditions, with the detachment of the oxide layer.

Figure 8(a–c) are the wear morphology of the original amorphous coatings, and amorphous coatings heat treated at 150°C and 250°C with the wear time of 30 min and the load of 20N in artificial seawater, respectively. It can be observed that the abrasive particles are reduced on the amorphous coatings heat treatment at 150 °C, the wear surface becomes uneven, accompanied by scratches, and the adhesion is obvious. Adhesive wear occurred at this time, and there was

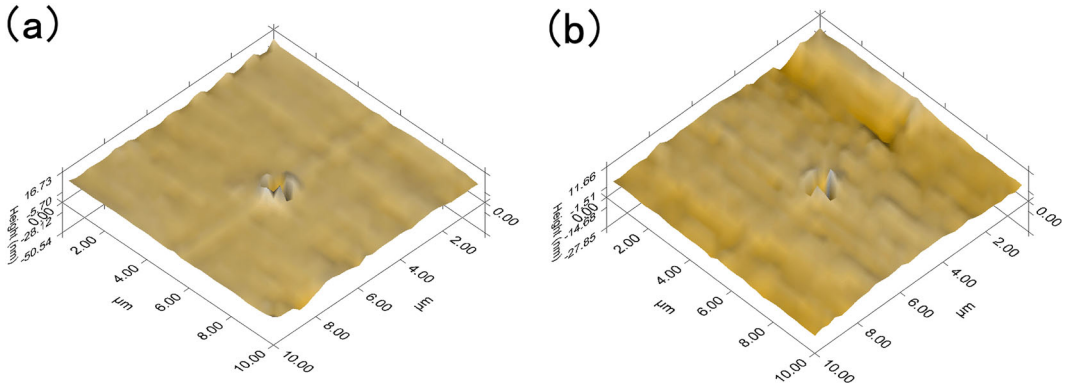

Figure 6. The creep indentation profile of the amorphous coatings heat-treated at 150°C (a) and 250°C (b) with the same holding time (30 s) and the same peak load (10mN).

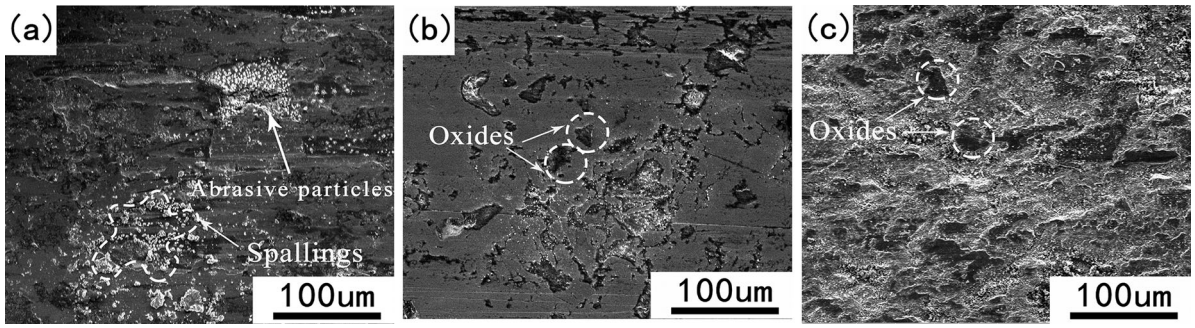

Figure 7. Surface wear morphology with 30 min wear time and 20N load: 304 stainless steel (a) and original amorphous coatings (b) in artificial seawater; (c) Original amorphous coatings in dry friction condition.

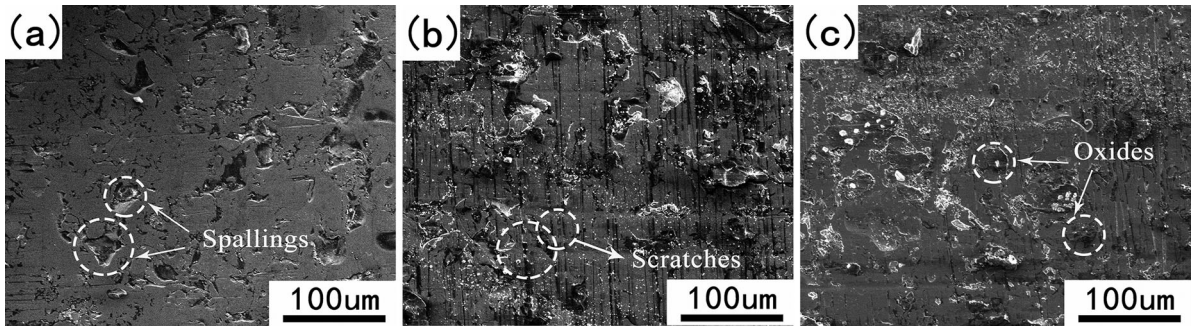

Figure 8. Surface wear morphology with 30 min wear time and 20 N load in artificial seawater: (a) Original coatings; 150°C (b) and 250°C (c) heat-treated amorphous coatings.

oxidative wear. The surface of the amorphous coatings treated at 250°C is smooth and flat, with a small amount of oxidation and abrasive particle. Its wear mechanism becomes oxidative wear with a small amount of abrasive wear. The original amorphous coatings peeling is relatively evacuated, mainly around the tiny holes of the amorphous coatings. The amorphous coatings are peeled off mainly around the tiny holes, because the crack around the tiny holes of the amorphous coatings will continue to expand until it breaks. This phenomenon is caused by repeated rubbing of the GCr15 steel ball on the amorphous coatings, and the residual stress is released. Finally, the surface layer is detached from the amorphous coatings in the form of a fragmented wear grindings and form a spalling pit [23]. Therefore, when amorphous coatings are annealed at a low temperature without crystallization, as the annealing temperature increases, the porosity decreases, which makes the wear resistance of the amorphous coating improved.

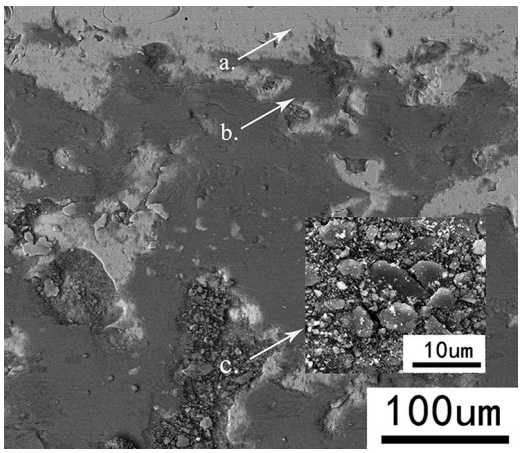

Figure 9. Wear morphology of amorphous coatings heat treated at 250°C in dry friction condition.

EDS analysis of the amorphous coatings

Figure 9 shows the EDS analysis of the wear surface of the amorphous coatings heat treated at 250°C in dry friction condition. The EDS element content distributions are reported in Table 2. The oxygen content in the white area is very low, considering that the error range of the instrument itself can be ignored. The oxygen content in the dark region b is up to 16.0 wt-%, because high frequency friction will significantly increase the surface temperature,

Table 2. Comparison of EDS element content in wear surface of amorphous coatings heat treated at 250°C in dry friction condition.

Element content (wt%)	Fe	O	Cr	Mo	C	B
Region a	55.1	0.4	25.6	17.1	1.9	0
Region b	68.7	16.0	9.3	4.9	1.1	0
Region c	75.0	16.5	4.8	2.0	1.6	0

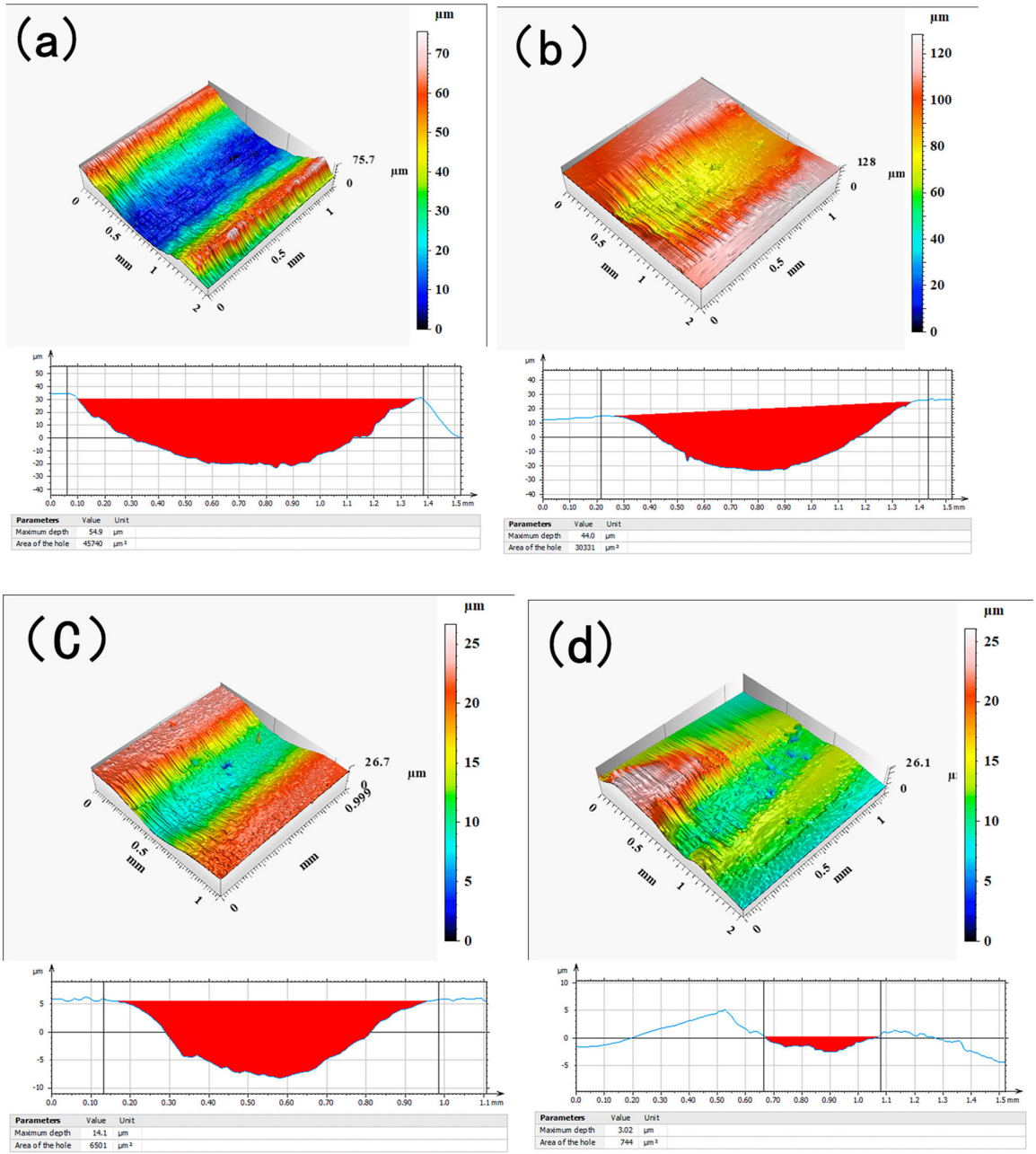

Figure 10. the three-dimensional topography of the surface wear under the applied load of 20 N at dry friction condition: (a) 304 stainless steel; (b) Original amorphous coatings; (c) 150°C heat-treated coatings; (d) 250°C heat-treated coatings.

and an oxide friction layer will be formed on the surface of the amorphous coatings. Therefore, the oxidative wear in dry friction and wear conditions is the main wear mechanism of the amorphous coatings [24]. The highest oxygen content in the c region is mainly oxidized wear debris, which indicates that the amorphous coatings is damaged and peeled under the mechanism of oxidative wear. The surface material transfer phenomenon occurs, and the residual stress is the main cause of cracking and spalling of the amorphous coatings [25].

Wear rate analysis of the amorphous coatings

The wear rate is calculated using the formula of $R_W = V_W/(S \times N)$ [26], where V_W is the wear volume (mm^3) drawn by the three-dimensional profiler, S is the sliding distance (m) and N is the load (N). Figure 10 shows a three-dimensional topographical view of the surface wear scar of 304 stainless steel (a), the original amorphous coatings (b) and heat-treated amorphous coatings at 150°C (c) and heat-treated amorphous coatings at 250°C (d) with 30 min wear time and 20N load in dry friction condition. It can be seen that the wear depth of 304 stainless steel is deeper than that of the amorphous coatings. By calculating the wear rate of 304 stainless steel (2.541E-4 $mm^3\ m^{-1}\ N$), it is 1.5 times the wear rate of original amorphous coatings (1.685E-4 $mm^3\ m^{-1}\ N$). Moreover, the wear rate of amorphous coatings is decreased through heat treatment, as shown in Table 3. Therefore, the amorphous coatings have a higher wear resistance than 304 stainless steel.

Table 3. Wear rate and wear scar roughness of the substrates and amorphous coatings with the same load (20 N) and the same wear time (30 min).

Specimen	Wear rate ($mm^3\ m^{-1}\ N$)	Wear scar roughness (μm)
Substrates	2.541E-4	6.021
Original amorphous coatings	1.685E-4	4.513
Heat-treated amorphous coatings at 150°C	3.611E-5	1.191
Heat-treated amorphous coatings at 250°C	4.3000E-6	1.044

Compared to the original amorphous coatings and substrates, the wear resistance of heat-treated amorphous coatings is better.

Conclusion

(1) XRD analysis shows that the structures of heat-treated Fe-based coatings are amorphous. As the heat treatment temperatures increase, the porosity of the amorphous coatings decreases, and the porosity of the heat-treat amorphous coatings at 250°C is the smallest. In artificial seawater, the amorphous coatings have better corrosion resistance than 304 stainless steel substrates, and the amorphous coatings heat treated at 250°C has the strongest corrosion resistance, which broadens the application of Fe-based amorphous coatings in marine corrosion protection.

(2) With the peak load of 6 and 10 mN, the same holding time of 10, 20 and 30 s, the creep displacements of amorphous coatings after heat-treated increase with the increase of loading time, but the increase of creep displacements of heat-treated amorphous coatings are smaller than that of the original amorphous coatings. Therefore, compared with the original amorphous coatings, the heat-treated coatings have great creep resistance, which means that the anti-deformation ability of the heat-treated Fe-based amorphous coatings is increased, and the service life of the Fe-based amorphous coatings is improved.

(3) Under dry friction condition, the wear rate of amorphous coatings decreases as heat-treat temperatures increasing, and the amorphous coatings heat-treated at 250°C has a minimum wear rate of 4.3000E-6 $mm^3\ m^{-1}$ N. Therefore, heat-treated amorphous coatings have better wear resistance. The amorphous coatings are less peeled off in artificial seawater than under dry friction conditions. In artificial seawater, the surface for amorphous coatings heat treated at 250°C is smoother and flatter than that of original coatings and heat treated at 150°C. These results indicate that the proper heat treatment process can improve the wear resistance of Fe-based amorphous coatings, which makes the service life of Fe-based amorphous coatings prolonged in the marine environment.

Disclosure statement

No potential conflict of interest was reported by the author(s).

Funding

This work is supported by the National Natural Science Foundation of China [51661016, 51861021, 51571105, 51661017]; Hongliu First-class Discipline Construction Plan of Lanzhou University of Technology.

References

[1] Sun YH. Inverse ductile–brittle transition in metallic glasses? Mater Sci Technol. 2015;31:635–650.
[2] Solomon I, Solomon N. Electrical, magnetic and thermal characterization of amorphous Fe-Co-Cr-B-Si alloys. Can Metall Quart. 2010;49:311–318.
[3] Zuo Y, Wang SL, Huang Y, et al. Corrosion resistance of Fe-based bulk amorphous alloy with sulfide inclusion. Acta Metall Sin-Engl. 2018;31:1098–1108.
[4] Lyphout C, Björklund S. Internal diameter HVAF spraying for wear and corrosion applications. J Therm Spray Technol. 2015;24:235–243.
[5] Li G, Gan YY, Liu CH, et al. Corrosion and wear resistance of Fe-based amorphous coatings. Coatings. 2020;10:73.
[6] Ma HR, Chen XY, Li JW, et al. Fe-based amorphous coating with high corrosion and wear resistance. Surf Eng. 2017;33:56–62.
[7] Miura H, Isa S, Omuro K, et al. Production of amorphous Fe-Ni based alloys by flame-spray quenching. Mater Trans JIM. 1981;22:597–606.
[8] Wang G, Chen J, Huang ZJ. Influence of spraying distance on microstructure and corrosion behavior of amorphous alloy coatings by thermal spraying. J Funct Mater. 2016;47:6185–6189.
[9] Branagan DJ, Swank WD, Meacham BE. Maximizing the glass fraction in iron-based high velocity oxy-fuel coatings. Metall Mater Trans A. 2009;40:1306–1313.
[10] Farmer J, Choi JS, Saw C, et al. Iron-based amorphous metals: high-performance corrosion-resistant material development. Metall Mater Trans A. 2009;40:1289–1305.
[11] Wu NC, Chen K, Sunb WH, et al. Correlation between particle size and porosity of Fe-based amorphous coating. Surf Eng. 2018;35:37–45.
[12] Zhang HJ, Gong YF, Zhang BT, et al. Corrosion and algal adhesion behaviors of HVOF-sprayed Fe-based amorphous coatings for marine applications. J Therm Spray Technol. 2019;28:283–290.
[13] Qin YJ, Wu YP, Zhang JF, et al. Optimization of the HOVF spray parameters by Taguchi method for high corrosion-resistant Fe-based coatings. J Mater Eng Perform. 2015;24:2637–2644.
[14] Li CY, Ding JQ, Zhu FP, et al. Indentation creep behavior of Fe-based amorphous coatings fabricated by high velocity Oxy-fue. J Non-Cryst Solids. 2018;503–504:62–68.

[15] Chen JC, Si H, Zhan WS, et al. Structural relaxation of amorphous alloys $Fei_{13.3}Ni_{69.6}B_{16.2}Si_{0.9}$. Acta Phys Sin. 1985;34:142–146.
[16] Fu YB. 含非晶涂层制备及其晶化规律研究 [Study on preparation and crystallization rules of containing amorphous coatings]. BJUT. 2009. China.
[17] Zhao YC, Mao RP, Yuan XP, et al. Corrosion behaviour of Ti-based bulk metallic glass matrix composites. J Mater Eng. 2018;46:25–30.
[18] Wang SL, Cheng JC, Yi SH, et al. Corrosion resistance of Fe-based amorphous metallic matrix coating fabricated by HVOF theral spraying. Trans Nonferrous Met Soc China. 2014;24:146–151.
[19] Souza CAC, Ribeiro DV, Kiminami CS. Corrosion resistance of Fe-Cr-based amorphous alloys: an overview. J Non-Cryst Solids. 2016; 442:56–66.
[20] Li XJ, Liu D, Liu Z, et al. Electrochemical performance of surface modification coatings on aluminum alloy in marine environment. Surf Technol. 2018;47:181–185.
[21] Peng J, Long ZL, Wei HQ, et al. Creep behavior of a Fe-based bulk amorphous alloy using nanoindentation. Acta Phys Sin. 2009;58:4059–4065.
[22] Venkateswarlu K, Rajinikanth V, Naveen T, et al. Abrasive wear behavior of thermally sprayed diamond reinforced composite coating deposited with both oxy-acetylene and HVOF techniques. Wear. 2009;266:995–1002.
[23] Zhang SQ, Du SM, Niu YP, et al. Friction and wear performances of Fe-based amorphous alloy coating. Lubr Eng. 2010;35:50–52.
[24] Ma HR, Li JW, Jiao J, et al. Wear resistance of Fe-based amorphous coatings prepared by AC-HVAF and HVOF. Mater Sci Technol. 2016;33:65–71.
[25] Pu CH, Xu BS, Wang HD, et al. Wear mechanism of 3Cr13 coating under accelerated condition of dry friction. Tribol. 2009;29:368–373.
[26] Gao H, Wei XS, Liang DD, et al. Friction and wear properties of HVAF sprayed Fe-based amorphous alloy coatings. Surf Technol. 2018;47:55–63.